Alternative photosynthesis pathways drive the algal CO_2-concentrating mechanism

https://doi.org/10.1038/s41586-022-04662-9

Received: 26 February 2021

Accepted: 18 March 2022

Published online: 27 April 2022

Check for updates

Adrien Burlacot[1,2], Ousmane Dao[1], Pascaline Auroy[1], Stephan Cuiné[1], Yonghua Li-Beisson[1] & Gilles Peltier[1]✉

Global photosynthesis consumes ten times more CO_2 than net anthropogenic emissions, and microalgae account for nearly half of this consumption[1]. The high efficiency of algal photosynthesis relies on a mechanism concentrating CO_2 (CCM) at the catalytic site of the carboxylating enzyme RuBisCO, which enhances CO_2 fixation[2]. Although many cellular components involved in the transport and sequestration of inorganic carbon have been identified[3,4], how microalgae supply energy to concentrate CO_2 against a thermodynamic gradient remains unknown[4–6]. Here we show that in the green alga *Chlamydomonas reinhardtii*, the combined action of cyclic electron flow and O_2 photoreduction—which depend on PGRL1 and flavodiiron proteins, respectively—generate a low luminal pH that is essential for CCM function. We suggest that luminal protons are used downstream of thylakoid bestrophin-like transporters, probably for the conversion of bicarbonate to CO_2. We further establish that an electron flow from chloroplast to mitochondria contributes to energizing non-thylakoid inorganic carbon transporters, probably by supplying ATP. We propose an integrated view of the network supplying energy to the CCM, and describe how algal cells distribute energy from photosynthesis to power different CCM processes. These results suggest a route for the transfer of a functional algal CCM to plants to improve crop productivity.

Microalgal photosynthesis in aquatic ecosystems has to overcome a low CO_2 availability resulting from the slow diffusion of CO_2 in water[7]. The CO_2-fixing enzyme RuBisCO has a low affinity[8] for CO_2, and thus the efficiency of algal photosynthesis is highly dependent on the CCM[9]. The algal CCM involves the sequential actions of inorganic carbon (C_i) transporters and carbonic anhydrases located in different cellular compartments[10], and results in active accumulation of CO_2 at the RuBisCO level[4,6]. Several CCM components have been identified in the green alga *C. reinhardtii*[3,4] (hereafter referred to as *Chlamydomonas*), particularly putative C_i transporters operating across the plasma membrane (high light activated 3[11] (HLA3)), the chloroplast envelope (low carbon inducible A[12,13] (LCIA)) and the thylakoid membrane (bestrophin-like transporters[14] (BSTs)). The C_i is eventually converted to CO_2 by a carbonic anhydrase[15] (CAH3), enabling its fixation by RuBisCO. The transport of C_i across membrane bilayers against a concentration gradient and its conversion to CO_2 are energy-dependent processes[6,14,16], and photosynthesis has a role in supplying the chemical energy required for the function of the CCM[17].

During photosynthesis, sunlight is converted to chemical energy by two photosystems (PSII and PSI) acting in series through the linear electron flow (LEF), reducing $NADP^+$ to NADPH and producing a pH gradient across the thylakoid membrane. The pH gradient is then leveraged for ATP synthesis, and both NADPH and ATP supply energy for CO_2 fixation. However, LEF produces less ATP than required for CO_2 fixation[18], and photosynthesis relies on additional mechanisms to rebalance this ratio[19]. These include (1) cyclic electron flow (CEF) around PSI, which involves both proton gradient regulation 5[20,21] (PGR5) and proton gradient regulation like 1[22,23] (PGRL1) proteins in plants and algae and (2) pseudo-cyclic electron flow (PCEF), which diverts electrons to O_2 at the PSI acceptor side[24], catalysed by flavodiiron proteins (FLVs) in cyanobacteria[25], bryophytes[26,27] and green microalgae[28]. Both CEF and PCEF generate a pH gradient without producing NADPH, thus re-equilibrating the high NADPH/ATP ratio of LEF. Another pathway involving several metabolic shuttles between chloroplast and mitochondria, which we designate chloroplast-to-mitochondria electron flow (CMEF), can also supply extra ATP for CO_2 fixation when CEF is deficient[29,30]. In this context, how photosynthesis energy is delivered to the different C_i transporters and how can this be done without compromising CO_2-fixation capacity are pivotal questions[4,6].

Here we have addressed these questions by studying *Chlamydomonas* mutants of the PGRL1-dependent CEF (*pgrl1*[23]), PCEF (*flvB*[28]) and BSTs[14]. We show that CCM activity is unaffected in single CEF or PCEF mutants but is severely impaired in double mutants and propose that the increased luminal proton concentration produced by the cooperative action of these mechanisms is used by CCM mechanisms operating downstream of BST thylakoid C_i transporters. We further establish that CMEF is involved in CCM functioning, most probably by supplying ATP to plasma membrane and/or chloroplast envelope C_i transporters, thus revealing how transport steps distant from the thylakoid can be powered.

[1]Aix Marseille Univ, CEA, CNRS, Institut de Biosciences et Biotechnologies Aix-Marseille, CEA Cadarache, Saint-Paul-lez-Durance, France. [2]Department of Plant Biology, Carnegie Institution for Science, Stanford, CA, USA. ✉e-mail: gilles.peltier@cea.fr

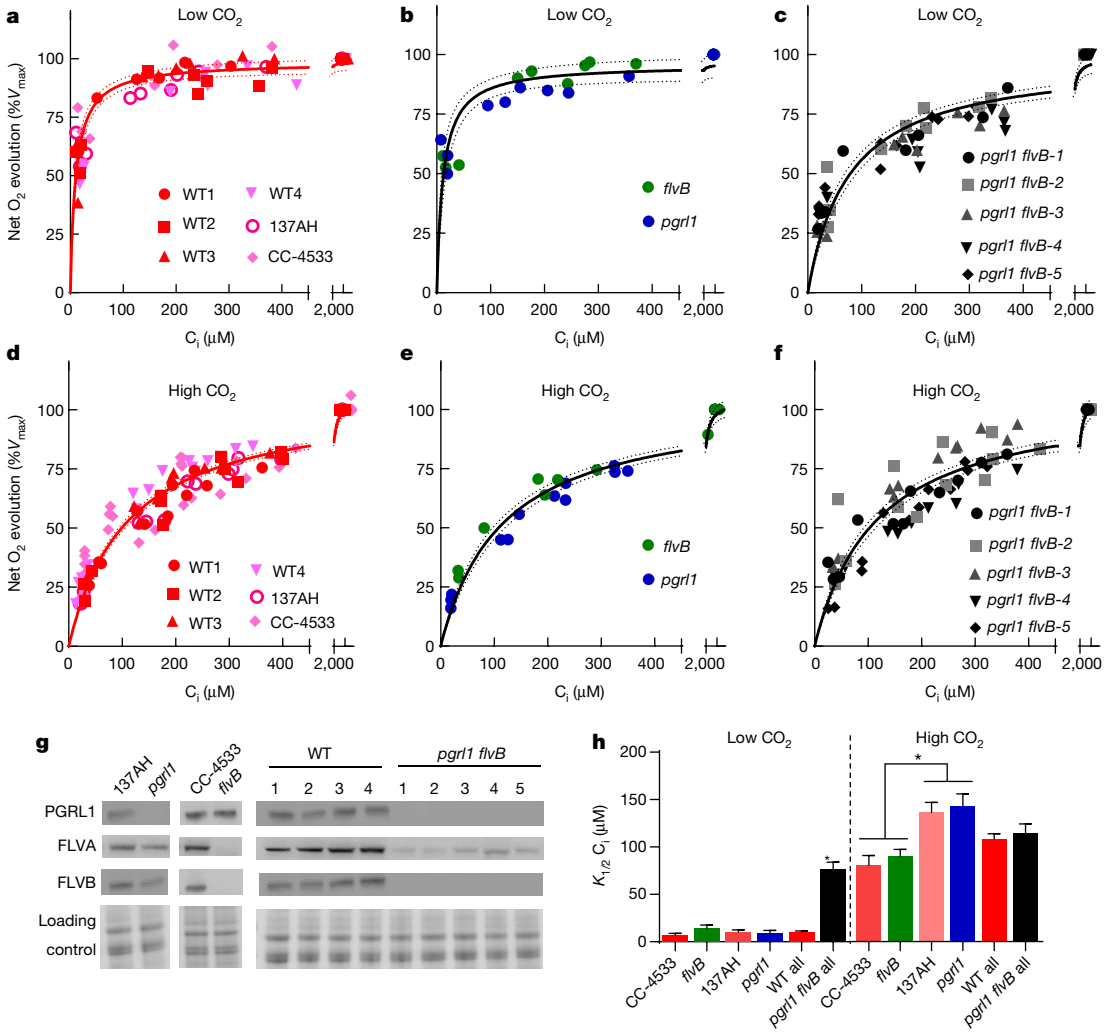

Fig. 1 | Deletion of PGRL1 and FLVB impairs photosynthetic affinity for C_i. **a**–**f**, Net O_2 production was measured at pH 7.2 in cells grown under air with 400 ppm (low CO_2) or 3% (high CO_2) CO_2. Shown are three replicates (dots) and hyperbolic fit (solid lines) with variability (dotted lines) for each strain. For each replicate, net O_2 production was measured following stepwise C_i addition, and normalized to the maximum photosynthetic net O_2 production. As these strains were generated in different genetic backgrounds (CC-4533 and 137AH) with contrasting photosynthetic activities (Extended Data Fig. 2a, c), the data are normalized to the V_{max}. **a**, **d**, 137AH and CC-4533 are the control strains for *pgrl1* and *flvB*, respectively. WT1–4 are four independent control strains obtained from the *pgrl1* × *flvB* crossing. **b**, **e**, *flvB* and *pgrl1* mutant strains. **c**, **f**, *pgrl1 flvB-1* to *pgrl1 flvB-5* are independent double-mutant strains. Data for each strain in **a**–**f** are from three biologically independent samples. **g**, Immunodetection of PGRL1, FLVA and FLVB in the different strains with Coomassie blue staining as loading control. **h**, $K_{1/2}$ values as determined from the hyperbolic fit for each strain. Data are mean ± s.d. of the fit of experimental data shown in **a**–**f** ($n = 3$ for single mutants and their controls), values for all double mutant strains (*pgrl1 flvB* all, $n = 15$) and their control strains (WT all, $n = 12$) have been pooled before fitting. *$P < 0.05$; one way ANOVA with Tukey correction.

Deletions of FLVs and PGRL1 impair C_i affinity

To investigate the involvement of FLV-dependent PCEF and PGRL1-dependent CEF in the energy supply to the CCM, we first measured net photosynthetic O_2 production at various C_i concentrations in *Chlamydomonas flvB*[28] or *pgrl1*[23] single mutants. When cells were grown under air (400 ppm CO_2 (low CO_2)), C_i affinities were similar for control wild-type (WT) strains and single mutants (half saturation constant ($K_{1/2}$) ≈ 10 µM), indicating a fully functional CCM (Fig. 1a, b, h). Under high CO_2 (air with 3% CO_2 supplementation), *flvB* and *pgrl1* mutants and their respective parental strains showed similar affinities for C_i, with a $K_{1/2}$ around 100 µM (Fig. 1d, e, h). To assess possible functional redundancy between FLVs and PGRL1, we obtained double mutants by genetic crossing of the single *pgrl1* and *flvB* mutants (Extended Data Fig. 1a). Among the progeny, we isolated five independent double mutants (*pgrl1 flvB-1*, *2*, *3*, *4* and *5*) as well as four independent control strains exhibiting normal accumulation of both FLVs and PGRL1 (WT1–4) (Fig. 1g, Extended Data Fig. 1). We observed no differences in C_i affinity between these strains when grown at high CO_2, but double mutants showed seven times lower affinity for C_i compared with control strains when grown at low CO_2 (Fig. 1c, f, h, Extended Data Fig. 2b, d).

Mutants defective in the CCM often cannot grow properly in low CO_2[31]. We compared growth at different CO_2 concentrations, pH and light intensities. Whereas all strains showed similar growth at high CO_2, the growth of *pgrl1 flvB* double mutants was impaired under low CO_2 and very low CO_2 (100 ppm CO_2 in air) (Fig. 2a), similar to the growth defect observed in the CCM-deficient mutant *cia5* (Fig. 2a, Extended Data Fig. 3). The growth defect observed in double mutants worsened with increasing light intensity but was barely affected by pH (Extended Data Fig. 3). The accumulation of the major CCM components, as evaluated by immunodetection, was similar in all strains, with the exception of LCI1, which was present at lower amounts in double mutants (Fig. 2b) and to a lesser extent in single mutants (Extended Data Fig. 4c). However, the fact that growth of the LCI1 knockout mutant is not affected[32]

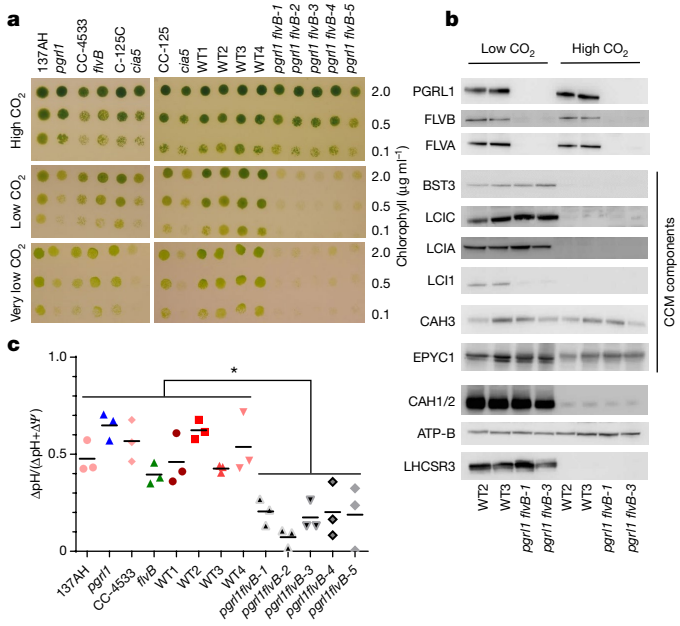

Fig. 2 | Growth of *pgrl1 flvB* double mutants is impaired at low CO_2 in the presence of CCM components. a, Growth tests for *pgrl1* and *flvB* mutants and the corresponding control strains (137AH and CC-4533, respectively) (left) and double mutants (*pgrl1 flvB-1* to *pgrl1 flvB-5*) and the corresponding control strains (WT1–4) (right). The *cia5* mutant was introduced as a CCM-deficient control together with its reference strain CC-125. Cells were spotted on plates containing minimal medium at pH 7.2 and grown under continuous illumination (60 µmol photon m^{-2} s^{-1}) under high CO_2, low CO_2 or very low CO_2 (100 ppm CO_2 in air). Spots shown are representative of ten independent experiments. **b**, Immunodetection of PGRL1, FLVA, FLVB and of the major CCM components in two independent *pgrl1 flvB* double mutants and controls grown under low or high CO_2. **c**, PMF partitioning between ΔpH and ΔΨ determined from electrochromic shift measurements. Horizontal lines show the mean and dots show individual replicates ($n = 3$ biologically independent sample). *pgrl1 flvB* double mutants showed a significantly lower pH gradient contribution to PMF than the single-mutant and control strains ($P < 0.05$, one way ANOVA).

at low CO_2, suggests that the lower LCI1 level observed in double *pgrl1 flvB* mutants is not the cause, but rather the consequence, of CCM misfunctioning. Carbonic anhydrase activity measured in vivo was induced at low CO_2, reaching similar levels in all strains (Extended Data Fig. 4f). Double mutants and control strains showed similar maximal O_2 photosynthetic production (Extended Data Fig. 2a, c) and PSII quantum yields (Extended Data Fig. 4a), as well as similar levels of major photosynthetic complexes (Extended Data Fig. 4b). Thus PGRL1-dependent CEF and FLV-dependent PCEF contribute to the CCM operation, and can compensate for each other, as exemplified by the absence of a CCM phenotype in single mutants. The growth impairment of the *pgrl1* mutant observed under high light indicates that the compensation by PCEF induces a metabolic imbalance that may affect growth on the long term, as previously proposed[29].

CCM uses luminal H^+ generated by CEF and PCEF

We hypothesized that PGRL1 and FLVs may generate an extra trans-thylakoid pH gradient that could provide energy for CCM. Whereas control strains and single *pgrl1* or *flvB* mutants generated both a similar pH gradient and proton motive force (PMF) as their control in light conditions (Fig. 2c, Extended Data Fig. 5), *pgrl1 flvB* double mutants were strongly impaired in their capacity to generate both pH gradient and PMF (Fig. 2c, Extended Data Fig. 5). It has been proposed[16] that luminal protons could be used during the last step of CCM to convert HCO_3^- to CO_2. Thus, to gain further insight into the link between CEF, PCEF and CCM energization, we assessed changes in the luminal proton concentration during CCM function in the different mutant strains. We monitored the level of the rapidly reversible component (qE) of the non-photochemical quenching of chlorophyll fluoresence (NPQ), which has recently been identified as a sensitive and reliable probe of luminal pH[33,34] (Fig. 3a) and depends on light-harvesting complex stress-related 3 protein (LHCSR3) accumulation in cells grown under low CO_2 (Fig. 2b, Extended Data Fig. 4c). In control lines, the NPQ level was highest when C_i level was low, and rapidly and reversibly decreased either in the light upon C_i injection or at low C_i when light was turned off (Fig. 3b; Extended Data Fig. 6a, c, e). We confirmed that state transitions (another NPQ component) did not contribute to CO_2-dependent NPQ changes (Extended Data Fig. 7a–c) and that the NPQ measured at low C_i is fully relaxed by the ionophore nigericin that suppresses the trans-thylakoidal pH gradient and can therefore be attributed to qE (Extended Data Fig. 7d–f, h, i). The CO_2-dependency of qE was not affected in single mutants. However, qE was not induced in *pgrl1 flvB* double mutants at low C_i (Fig. 3c, Extended Data Fig. 6f, h), although these strains accumulated normal amounts of LHCSR3 (Fig. 2b) and maintained the capacity to induce substantial qE upon medium acidification (Extended Data Fig. 6i, j), which is consistent with the incapacity of the *pgrl1 flvB* double mutants to generate a pH gradient (Fig. 2c). We conclude from this experiment that CEF and PCEF contribute to energize the CCM through the generation of a low luminal pH, with both mechanisms being able to substitute for each other in single mutants.

Three BST-like proteins have been proposed to transport C_i at the thylakoid level[14]. To gain insight into the role of the luminal proton concentration in the CCM functioning, we assessed the kinetics of the NPQ in a BST-knockdown strain[14] (*bsti-1*) in response to repetitive C_i supply. *bsti-1* was found to accumulate variable levels of LHCSR3 depending on the growth conditions (Extended Data Fig. 4e)—we thus selected conditions under which accumulation of LHCSR3 was close to that in the control strain. Whereas the control strain showed a NPQ decrease for each C_i injection followed by an increase upon C_i depletion (Fig. 3d), the NPQ of *bsti-1* was barely affected (Fig. 3e). We validated that *bsti-1* displays a NPQ component attributable to qE and is able to generate a pH gradient similar to the control strain (Extended Data Figs. 5, 7g). In sum, *bsti-1* is able to generate a pH gradient and a low luminal pH but it is unable to use it to accumulate C_i.

CMEF energizes distant C_i transporters

To gain quantitative insight into the nature of compensation mechanisms in *pgrl1*, we investigated the C_i-dependence of the light-dependent O_2 consumption measured using ^{18}O-labelled O_2. As previously reported[35,36], O_2 consumption increased at low C_i in control strains (Extended Data Fig. 8a, e). In *pgrl1*, O_2 uptake rates were higher than in control strains (Extended Data Fig. 8a–d), which is consistent with a compensation of a defect in CEF by PCEF[29]. O_2 uptake rates were strongly diminished in *flvB*[28], but surprisingly, a C_i-dependent O_2 uptake process remained (Extended Data Fig. 8e, f). To determine whether mitochondrial respiration is responsible for the remaining light-dependent O_2 uptake, we used two mitochondrial respiration inhibitors, myxothiazol and salicyl hydroxamic acid (SHAM), which inhibit the cytochrome bc_1 complex and the mitochondrial alternative oxidase, respectively. We show that the remaining light-dependent O_2 uptake measured at low C_i in *flvB* is indeed owing to mitochondrial respiratory activity driven by photosynthesis and therefore attributed to CMEF (Extended Data Fig. 8k).

We then investigated the contribution of mitochondria to CCM energization in WT strains. Whereas addition of respiratory inhibitors had no effect on the maximal net O_2 production rate (V_{max}) and C_i affinity of high CO_2-grown strains ($K_{1/2} \approx 100$ µM) (Extended Data Fig. 9d–f, l, m), it reduced the C_i affinity of low CO_2-grown control strains by half ($K_{1/2} > 20$ µM) compared with untreated cells ($K_{1/2} \approx 10$ µM) (Fig. 3f). The

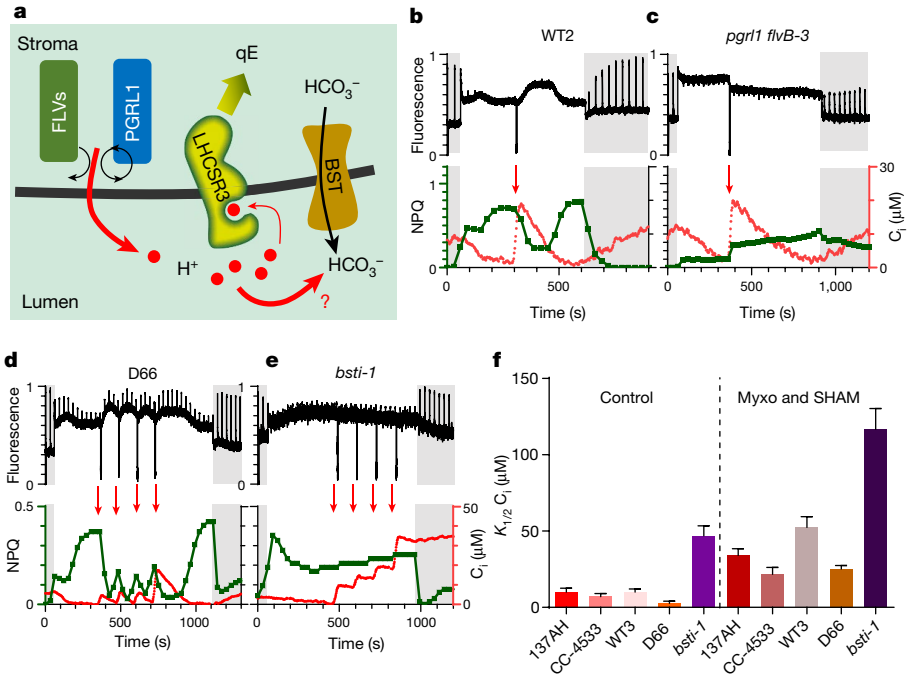

Fig. 3 | CEF, PCEF and CMEF contribute energy to the CCM. a, Schematic view describing the principle of using the qE component of NPQ to probe changes in luminal pH during CCM function. **b**–**e**, Combined measurements of chlorophyll fluorescence (top panels), C_i concentrations and NPQ (bottom panels) during dark–light–dark transitions in WT2 (**b**), *pgrl1 flvB-3* (**c**), the *bsti-1* control strain D66 (**d**) and *bsti-1* (**e**). All strains were grown at low CO_2. Results are from representative experiments ($n = 3$ biologically independent samples). Red arrows indicate stepwise addition of bicarbonate. **f**, Inhibitors of mitochondrial respiration decrease the phosynthetic affinity for C_i in cells grown under low CO_2. Net photosynthetic O_2 production was measured as in Fig. 1. $K_{1/2}$ values were determined from hyperbolic fits for the different strains in the presence or absence of the mitochondrial inhibitors myxothiazol (Myxo, 2.5 µM) and SHAM (400 µM), which act on the cytochrome bc_1 complex and the alternative oxidase, respectively. Data are mean values ± s.d. of the fit of data shown in Extended Data Fig. 9a–c, g, h. When grown under low CO_2 and treated with myxothiazol and SHAM, all WT and mutant strains produced $K_{1/2}$ values that were significantly different compared with non-treated strains ($P < 0.05$; one way ANOVA with Tukey correction).

effect on C_i affinity was observed only when myxothiazol and SHAM were added together (Extended Data Fig. 10), indicating that both alternative oxidase and cytochrome bc_1 electron pathways contribute to CCM energization. Notably, respiratory inhibitors also increased the $K_{1/2}$ of the air-grown *bsti-1* mutant (Fig. 3f, Extended Data Fig. 9h), thus showing that the contribution of mitochondria to CCM energization operates at the level of transporters distant from the thylakoids. The contribution of the different pathways (CEF, PCEF and CMEF) was deduced from O_2 consumption rates measured in the different mutants during C_i depletion (Extended Data Fig. 8). Whereas the contribution of the PGRL1-dependent CEF remained relatively constant, the contribution of FLV-dependent PCEF and CMEF increased markedly at low C_i (Fig. 4a).

Discussion

Although the requirement of the CCM for energy from photosynthesis has been long recognized[17], the associated molecular mechanisms have remained poorly understood[4]. The participation of PCEF[36] or CEF[37] has been proposed, but their actual and respective contributions have not been established. Here we demonstrate that both FLV-dependent PCEF and PGRL1-dependent CEF cooperate to supply energy to the CCM by the generation of a pH gradient. Moreover, we propose that the low luminal pH generated by both mechanisms is used by a thylakoid-localized CCM process linked to the functioning of BSTs. Because mammalian BSTs[38] are Cl^- channels that are highly permeable to HCO_3^-, protons that accumulates in the lumen from the combined actions of CEF and PCEF are probably used for the conversion of HCO_3^- to CO_2 mediated by CAH3, and the PMF generated by both mechanisms (Extended Data Fig. 5) is likely to favour HCO_3^- translocation through BSTs (Fig. 4b).

We further establish that mitochondrial respiration, whose role in CCM energization has been largely ignored, provides energy to CCM transporters that are distant from the thylakoids through efficient inter-organelle redox trafficking. From the analysis of the respective contribution of each mechanism as a function of C_i concentration, we conclude that whereas the contribution of CEF is relatively constant, the contribution of PCEF increases at low C_i concentrations, and that of CMEF also becomes important at the lowest C_i concentrations. As these are typical conditions in which putative ATP-dependent periplasmic and chloroplast envelope transporters (HLA3 and LCIA, respectively) are highly active[4,12,13], we propose that the ATP produced by CMEF at low C_i supplies energy to one or both transporters (Fig. 4). The lower growth decrease observed for *pgrl1 flvB* mutants at very low CO_2 (Extended Data Fig. 3d–f) indicates that external transporters (HLA3 and/or LCIA), which depend on the CMEF energy supply, may be the prime drivers of the CCM in these conditions. Of note, LCI1 accumulation, whose function is tightly linked to HLA3[3,32], decreased in *pgrl1*, *flvB*, *pgrl1 flvB* and *bsti-1*, indicating that an impairment of the CCM at the thylakoid level may regulate periplasmic transport processes mediated by LCI1. This could be owing to an increased cytosolic C_i concentration resulting from the absence of functional thylakoid C_i transport, which would in turn trigger down-regulation of LCI1 expression to avoid cytosolic C_i over-accumulation.

The presence of an active CCM is a key factor influencing phytoplankton biomass production in the oceans[2], especially for phytoplankton species producing large oceanic blooms[39]. However, the lack of knowledge about CCM activity in situ[9] makes it difficult to predict how global changes will affect phytoplankton communities[40]. We demonstrate here that the presence of a functional CCM can be probed by measuring C_i-dependent NPQ, which could be used as a simple parameter to determine CCM activity in aquatic ecosystems.

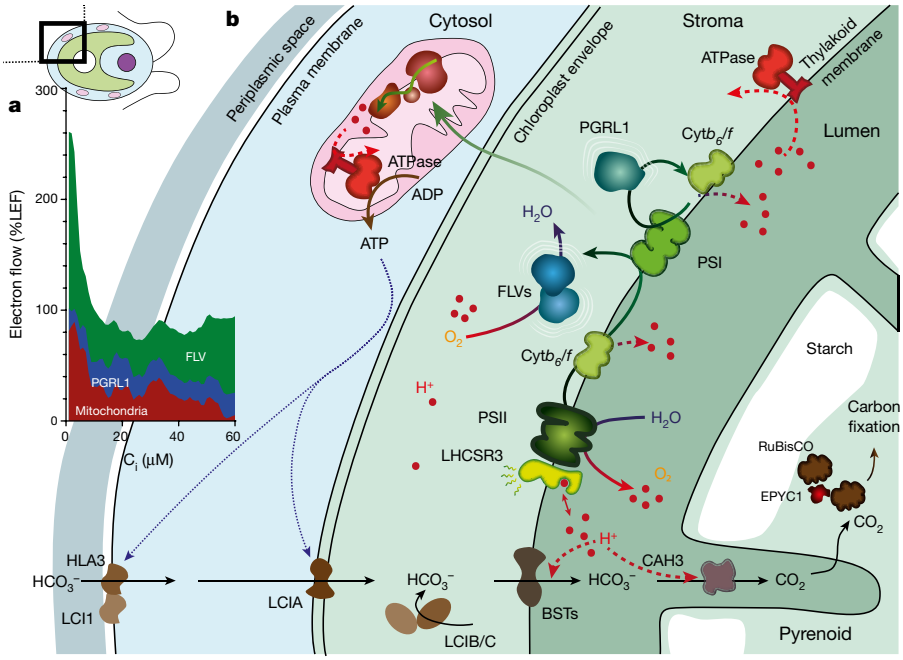

Fig. 4 | Proposed mechanism of the CCM-energization network in algal cells. a, Contributions of FLV-dependent PCEF, PGRL1-dependent CEF and CMEF to CCM energization at different C_i concentrations were quantified from O_2 exchange measurements performed in the different mutant strains and expressed as a percentage of LEF (Extended Data Fig. 8). **b**, Schematic view of the CCM-energization network. CCM components including LCI1, HLA3, LCIA and BST transporters, LCIB, LCIC, CAH3, EYPC1 and RuBisCO are shown in brown, and components of the photosynthetic electron transport chain (PSII, PSI, Cytb_6/f) are in green. We propose here that luminal protons generated by the combined action of FLV-dependent PCEF and PGRL1-dependent CEF are used to convert bicarbonate to CO_2 downstream of BST anionic channels. CMEF would generate the ATP needed to power C_i transporters distant from the thylakoid, such as LCIA and HLA3.

A potential limitation of a thylakoid CCM process consuming the luminal protons would be competition with the synthesis of ATP required for CO_2 fixation[14]. This is particularly critical as LEF is known to supply less ATP than is required for CO_2 fixation[19]. We suggest here that the combined action of the three alternative mechanisms, CEF, PCEF and CMEF, all of which result in an increase of the ATP/NADPH ratio, can fulfill the energy requirement of the CCM without compromising CO_2 fixation. A major biotechnological challenge in CCM research is the improvement of crop productivity by transferring microalgal components to higher plants[41–43]. Building a fully functional CCM in plants represents a tremendous scientific challenge, which has recently regained considerable interest[4,44]. Our study shows that an integrated understanding of the cellular energetics is key towards fulfilling the energy requirement of a synthetic CCM without compromising the efficiency of photosynthetic CO_2 fixation. For instance, the expression of FLVs in higher plants, which has been shown to supply extra PMF during photosynthesis[45–48], appears as a promising starting point to supply the extra energy needed to power thylakoid C_i transport. We foresee that future research coupling energy source and CCM expression should help to boost plant productivity.

Online content

Any methods, additional references, Nature Research reporting summaries, source data, extended data, supplementary information, acknowledgements, peer review information; details of author contributions and competing interests; and statements of data and code availability are available at https://doi.org/10.1038/s41586-022-04662-9.

1. Field, C. B., Behrenfeld, M. J., Randerson, J. T. & Falkowski, P. Primary production of the biosphere: integrating terrestrial and oceanic components. *Science* **281**, 237–240 (1998).
2. Mackey, K. R., Morris, J. J., Morel, F. M. & Kranz, S. A. Response of photosynthesis to ocean acidification. *Oceanography* **28**, 74–91 (2015).
3. Mackinder, L. C. M. et al. A spatial interactome reveals the protein organization of the algal CO_2-concentrating mechanism. *Cell* **171**, 133–147.e114 (2017).
4. Mackinder, L. C. M. The *Chlamydomonas* CO_2-concentrating mechanism and its potential for engineering photosynthesis in plants. *New Phytol.* **217**, 54–61 (2018).
5. Raven, J. A. Inorganic carbon acquisition by eukaryotic algae: four current questions. *Photosynth. Res.* **106**, 123–134 (2010).
6. Raven, J. A., Beardall, J. & Giordano, M. Energy costs of carbon dioxide concentrating mechanisms in aquatic organisms. *Photosynth. Res.* **121**, 111–124 (2014).
7. Maberly, S. C. & Gontero, B. Ecological imperatives for aquatic CO_2-concentrating mechanisms. *J. Exp. Bot.* **68**, 3797–3814 (2017).
8. Savir, Y., Noor, E., Milo, R. & Tlusty, T. Cross-species analysis traces adaptation of Rubisco toward optimality in a low-dimensional landscape. *Proc. Natl Acad. Sci. USA* **107**, 3475–3480 (2010).
9. Reinfelder, J. R. Carbon concentrating mechanisms in eukaryotic marine phytoplankton. *Annu. Rev. Mar. Sci.* **3**, 291–315 (2011).
10. Moroney, J. V. et al. The carbonic anhydrase isoforms of *Chlamydomonas reinhardtii*: intracellular location, expression, and physiological roles. *Photosynth. Res.* **109**, 133–149 (2011).
11. Duanmu, D., Miller, A. R., Horken, K. M., Weeks, D. P. & Spalding, M. H. Knockdown of limiting-CO_2-induced gene HLA3 decreases HCO_3^- transport and photosynthetic C_i affinity in *Chlamydomonas reinhardtii*. *Proc. Natl Acad. Sci. USA* **106**, 5990–5995 (2009).
12. Wang, Y. & Spalding, M. H. Acclimation to very low CO_2: contribution of limiting CO_2 inducible proteins, LCIB and LCIA, to inorganic carbon uptake in *Chlamydomonas reinhardtii*. *Plant Physiol.* **166**, 2040–2050 (2014).
13. Yamano, T., Sato, E., Iguchi, H., Fukuda, Y. & Fukuzawa, H. Characterization of cooperative bicarbonate uptake into chloroplast stroma in the green alga *Chlamydomonas reinhardtii*. *Proc. Natl Acad. Sci. USA* **112**, 7315–7320 (2015).
14. Mukherjee, A. et al. Thylakoid localized bestrophin-like proteins are essential for the CO_2 concentrating mechanism of *Chlamydomonas reinhardtii*. *Proc. Natl Acad. Sci. USA* **116**, 16915–16920 (2019).
15. Karlsson, J. et al. A novel α-type carbonic anhydrase associated with the thylakoid membrane in *Chlamydomonas reinhardtii* is required for growth at ambient CO_2. *EMBO J.* **17**, 1208–1216 (1998).
16. Raven, J. A. CO_2-concentrating mechanisms: a direct role for thylakoid lumen acidification? *Plant Cell Environ.* **20**, 147–154 (1997).
17. Badger, M. R., Kaplan, A. & Berry, J. A. Internal inorganic carbon pool of *Chlamydomonas reinhardtii*. *Plant Physiol.* **66**, 407–413 (1980).
18. Allen, J. F. Photosynthesis of ATP—electrons, proton pumps, rotors, and poise. *Cell* **110**, 273–276 (2002).
19. Allen, J. F. Cyclic, pseudocyclic and noncyclic photophosphorylation: new links in the chain. *Trends Plant Sci.* **8**, 15–19 (2003).
20. Munekage, Y. et al. PGR5 is involved in cyclic electron flow around photosystem I and is essential for photoprotection in *Arabidopsis*. *Cell* **110**, 361–371 (2002).

21. Johnson, X. et al. Proton gradient regulation 5-mediated cyclic electron flow under ATP- or redox-limited conditions: a study of Δ*ATPase pgr5* and Δ*rbcL pgr5* mutants in the green alga *Chlamydomonas reinhardtii*. *Plant Physiol.* **165**, 438–452 (2014).
22. DalCorso, G. et al. A complex containing PGRL1 and PGR5 is involved in the switch between linear and cyclic electron flow in *Arabidopsis*. *Cell* **132**, 273–285 (2008).
23. Tolleter, D. et al. Control of hydrogen photoproduction by the proton gradient generated by cyclic electron flow in *Chlamydomonas reinhardtii*. *Plant Cell* **23**, 2619–2630 (2011).
24. Curien, G. et al. The water to water cycles in microalgae. *Plant Cell Physiol.* **57**, 1354–1363 (2016).
25. Helman, Y. et al. Genes encoding a-type flavoproteins are essential for photoreduction of O_2 in cyanobacteria. *Curr. Biol.* **13**, 230–235 (2003).
26. Gerotto, C. et al. Flavodiiron proteins act as safety valve for electrons in *Physcomitrella patens*. *Proc. Natl Acad. Sci. USA* **113**, 12322–12327 (2016).
27. Shimakawa, G. et al. The Liverwort, *Marchantia*, drives alternative electron flow using a flavodiiron protein to protect PSI. *Plant Physiol.* **173**, 1636–1647 (2017).
28. Chaux, F. et al. Flavodiiron proteins promote fast and transient O_2 photoreduction in *Chlamydomonas*. *Plant Physiol.* **174**, 1825–1836 (2017).
29. Dang, K. V. et al. Combined increases in mitochondrial cooperation and oxygen photoreduction compensate for deficiency in cyclic electron flow in *Chlamydomonas reinhardtii*. *Plant Cell* **26**, 3036–3050 (2014).
30. Bailleul, B. et al. Energetic coupling between plastids and mitochondria drives CO_2 assimilation in diatoms. *Nature* **524**, 366 (2015).
31. Wang, Y., Stessman, D. J. & Spalding, M. H. The CO_2 concentrating mechanism and photosynthetic carbon assimilation in limiting CO_2: how *Chlamydomonas* works against the gradient. *Plant J.* **82**, 429–448 (2015).
32. Kono, A. & Spalding, M. H. LCI1, a *Chlamydomonas reinhardtii* plasma membrane protein, functions in active CO_2 uptake under low CO_2. *Plant J.* **102**, 1127–1141 (2020).
33. Bonente, G. et al. Analysis of LhcSR3, a protein essential for feedback de-excitation in the green alga *Chlamydomonas reinhardtii*. *PLoS Biol.* **9**, e1000577 (2011).
34. Tian, L. et al. pH dependence, kinetics and light-harvesting regulation of nonphotochemical quenching in *Chlamydomonas*. *Proc. Natl Acad. Sci. USA* **116**, 8320–8325 (2019).
35. Sültemeyer, D. F., Klug, K. & Fock, H. P. Effect of dissolved inorganic carbon on oxygen evolution and uptake by *Chlamydomonas reinhardtii* suspensions adapted to ambient and CO_2-enriched air. *Photosynth. Res.* **12**, 25–33 (1987).
36. Sültemeyer, D., Biehler, K. & Fock, H. P. Evidence for the contribution of pseudocyclic photophosphorylation to the energy requirement of the mechanism for concentrating inorganic carbon in *Chlamydomonas*. *Planta* **189**, 235–242 (1993).
37. Lucker, B. & Kramer, D. M. Regulation of cyclic electron flow in *Chlamydomonas reinhardtii* under fluctuating carbon availability. *Photosynthesis Res.* **117**, 449–459 (2013).
38. Qu, Z. & Hartzell, H. C. Bestrophin Cl^- channels are highly permeable to HCO_3^-. *Am. J. Physiol. Cell Physiol.* **294**, C1371–C1377 (2008).
39. Rost, B., Riebesell, U., Burkhardt, S. & Sültemeyer, D. Carbon acquisition of bloom-forming marine phytoplankton. *Limnol. Oceanogr.* **48**, 55–67 (2003).
40. Basu, S. & Mackey, K. R. M. Phytoplankton as key mediators of the biological carbon pump: their responses to a changing climate. *Sustainability* **10**, 869 (2018).
41. Atkinson, N. et al. Introducing an algal carbon-concentrating mechanism into higher plants: location and incorporation of key components. *Plant Biotechnol. J.* **14**, 1302–1315 (2016).
42. Meyer, M. T., McCormick, A. J. & Griffiths, H. Will an algal CO_2-concentrating mechanism work in higher plants? *Curr. Opin. Plant Biol.* **31**, 181–188 (2016).
43. Nölke, G. et al. The integration of algal carbon concentration mechanism components into tobacco chloroplasts increases photosynthetic efficiency and biomass. *Biotechnol. J.* **14**, 1800170 (2019).
44. Hennacy, J. H. & Jonikas, M. C. Prospects for engineering biophysical CO_2 concentrating mechanisms into land plants to enhance yields. *Annu. Rev. Plant Biol.* **71**, 461–485 (2020).
45. Yamamoto, H., Takahashi, S., Badger, M. R. & Shikanai, T. Artificial remodelling of alternative electron flow by flavodiiron proteins in Arabidopsis. *Nat. Plants* **2**, 16012 (2016).
46. Wada, S. et al. Flavodiiron protein substitutes for cyclic electron flow without competing CO_2 assimilation. *Plant Physiol.* **176**, 1509–1518 (2017).
47. Gómez, R. et al. Faster photosynthetic induction in tobacco by expressing cyanobacterial flavodiiron proteins in chloroplasts. *Photosynth. Res.* **136**, 129–138 (2018).
48. Vicino, P. et al. Expression of flavodiiron proteins Flv2–Flv4 in chloroplasts of *Arabidopsis* and tobacco plants provides multiple stress tolerance. *Int. J. Mol. Sci.* **22**, 1178 (2021).

Methods

Chlamydomonas flvB, *pgrl1* and *bsti-1* mutants and their respective parental strains CC-4533, 137AH and D66 were previously described[14,23,28]. All strains were grown phototrophically under moderate light (80 µmol photons $m^{-2} s^{-1}$) in minimal medium either under low CO_2 or high CO_2. Gas exchange rates were measured using a membrane inlet mass spectrometer[49] and combined NPQ measurements were done as previously described[50]. All replicates shown are biological replicates from independent cultures. All data fitting, analysis, and plotting has been made using GraphPad Prism (v.6.07).

Chlamydomonas strains and cultivation

All *Chlamydomonas* strains were grown photo-autotrophically in 150-ml flasks at 25 °C in a buffered minimal medium (20 mM MOPS pH = 7.2) under constant illumination (80 µmol photons $m^{-2} s^{-1}$). Cells were collected during the exponential phase. The mt^+ *flvB-21* mutant generated in ref. [51] was crossed with the mt^- *pgrl1* mutant, and the progenies were screened based on chlorophyll fluorescence transients for *FLVB* insertion and PCR for *PGRL1* insertion (Extended Data Fig. 2b, c). Five independent strains exhibiting a *flvB* mutant-like chlorophyll fluorescence transient[50] and harbouring an insertion of the paromomycin cassette at the *PGRL1* locus were selected (Extended Data Fig. 2d). Four independent strains exhibiting WT chlorophyll fluorescence phenotype and no insertion at the *PGRL1* locus were selected as control strains (Extended Data Fig. 2d). The absence of FLVB and PGRL1 proteins in the five independent double mutants (named *pgrl1 flvB-1*, *-2*, *-3*, *-4*, and *-5*) and their presence in the four independent control strains (named WT1, 2, 3 and 4) was confirmed by immunodetection (Fig. 1g). The *bsti-1* mutant and its control strain D66 have been described[14].

DNA extractions and PCR amplification

Total DNA was extracted by mixing one cell colony in 50 µl of a 10 mM Na-EDTA (Sigma-Aldrich) solution. Putative insertion in the *PGRL1* locus was confirmed in progeny of the crossing by PCR using *dreemTaq* DNA polymerase with green GC Buffer (Thermo Scientific). The two primer sequences used to amplify the *PRGL1* locus were: 5′-TTACGCAGCGGCCTTAGCCTTCTTCTTGGC-3′ and 5′-GGCTAAGCGCTGTGTGCCGC-3′. PCR cycles were: 2 min at 95 °C for 40 cycles: 30 s at 95 °C, 30 s at 60 °C, 2 min at 72 °C, and 4 min at 72 °C for final extension. PCR products were separated on 1% (w/v) agarose gels.

Immunoblot analysis

For protein analysis, 10^6 exponentially growing cells (approximately 10 µg chlorophyll per ml) were collected by centrifugation at 4,000*g* for 3 min at 4 °C. Pellets were resuspended in 200 µl of 1% SDS and 800 µl of cold acetone was added to extract chlorophyll and incubated for 30 min at −20 °C. Samples were then centrifuged for 10 min, 16,000*g* at 4 °C and chlorophyll concentration measured on the supernatant. The protein pellet was resuspended with Novex Nupage LDS buffer 1× (Invitrogen), and proteins were then denaturated at 70 °C for 20 min. Protein extracts (10 µg protein) were loaded on Novex Nupage Bis tris 12% (Invitrogen) gel, run 1 h at 190 V in Novex Nupage (Invitrogen) MOPS buffer or MES (for PsaC) buffers and transferred to nitrocellulose membrane (or PVDF for LCIC) using semidry transfer technique. Immunodetection was performed using antibodies raised against PGRL1 (1:1,000)[23], FLVB (1:1,000) and FLVA (1:1,000)[28], NDA2 (1:5,000)[52]. Other antibodies against PsbD (AS06 146, 1:10,000), PsaC (AS10 939, 1:1,000), Cytb6 (AS03-034, 1:10,000), RbcL (AS03 037, 1:5,000), ATP-B (AS05-085, 1:5,000), COXIIB (AS06 151, 1:5,000), AOX1 (AS06 152, 1:2,000), FeSOD (AS06-125, 1:1,000), EPYC1 (AS09-602, 1:500), LHCSR3 (AS14-2766, 1:500), CAH1/2 (AS11-1737, 1:1,000) and CAH3 (AS05 073, 1:2,000) were obtained from Agrisera (https://www.agrisera.com/). The LCIC antibody (1:1,000) was generated against a synthetic peptide containing the sequence of 12 amino acids found in the C-terminus of LCIC as described[53]. Two rabbits were injected with the synthetic peptide for the production of LCIC antibody. BST3 (1:500, dilution) antibody was a gift from L. Mackinder, LCI1 (1:500, dilution) and LCIA (1:2,500, dilution) antibodies was a gift from H. Fukuzawa. Unless otherwise stated, PageRuler (ThermoFisher) was used as the molecular weight ladder. Uncropped and unprocessed scans of the blots shown in this study are visible in source data.

Growth tests

The different *Chlamydomonas* strains were cultivated at 400 ppm CO_2 (low CO_2), except *cia5* and CC125 which were grown under 3% CO_2 (high CO_2) and acclimatized to low CO_2 for 24 h before spotting as described[12], because the *cia5* mutant is unable to grow[54] autotrophically without high CO_2. Cells were collected during exponential growth and resuspended in fresh minimal medium to 0.1, 0.5 or 2 µg chlorophyll per ml. Eight-microlitre drops were spotted on plates at pH = 7.2 or 8.2 (buffered with 20 mM MOPS or Tris, respectively) and exposed to high CO_2, low CO_2 or very low CO_2. Homogeneous light was supplied by a panel of fluorescent tubes, and neutral filters were used to obtain the desired light intensity. Temperature was maintained at 25 °C at the level of plates by means of fans.

CO_2 affinity of net O_2 photosynthesis

CO_2 affinity was determined using membrane inlet mass spectrometry[49] (MIMS). Cells grown at air level or 3% CO_2 were collected, centrifuged at 450 *g* for 3 min and resuspended in fresh minimal medium (pH = 7.2) at 10 µg chlorophyll per ml. The cell suspension was then bubbled in the MIMS reaction vessel with a CO_2 depleted gas mixture (80 % N_2, 20 % O_2). Upon CO_2 depletion, the reaction vessel was closed, light was turned on (2,000 µmol photons $m^{-2} s^{-1}$; green LEDs) and gas exchange recorded. Increasing amounts of bicarbonate were then sequentially added to reach various C_i concentrations inside the reaction vessel during gas exchange measurements.

Carbonic anhydrase activity measurements

Carbonic anhydrase activity was determined in intact cells by monitoring $^{18}O/^{16}O$ isotope exchange between ^{18}O-enriched CO_2 and H_2O using MIMS as described[49]. Doubly labelled $^{13}C^{18}O_2$ was prepared by equilibrating 1 M $NaH^{13}CO_3$ (99% ^{13}C-atom, Euriso-top) with $H_2{}^{18}O$ (97 % ^{18}O-atom, Cambridge Isotope Lab.) for 24 h at room temperature. The reaction vessel (1.5 ml) contained minimal growth medium buffered with 20 mM MOPS (pH 7.2). At $t = 0$, 15 µl of a 1 M $NaH^{13}C^{18}O_3$ solution were added and the isotope exchange was measured by continuously recording the concentration of $^{13}C^{18}O^{18}O$ ($m/z = 49$), $^{13}C^{18}O^{16}O$ ($m/z = 47$) and $^{13}C^{16}O^{16}O$ ($m/z = 45$). CO_2 unlabelling was followed by determining the time constant of the isotope content decrease[49,55,56], first for 3 min in the absence of algae, and then for 3 min following addition of the algal sample (20 µl at 50 µg chlorophyll per ml). Total carbonic anhydrase activity of the algal sample was expressed on a chlorophyll content basis, as the time constant of the isotope content decrease, after subtracting the exchange activity measured in the absence of algae.

Electrochromic shift measurement

Electrochromic shift (ECS) was assessed by measuring the absorbance changes of cells at 520 and 545 nm using a JTS-100 spectrophotometer (BioLogic). Cells were collected in exponential phase, centrifuged, and resuspended at around 150 µg chlorophyll per ml in minimal growth medium buffered with 20 mM MOPS (pH 7.2) with a final concentration of 2 mM HCO_3^-. The cell suspension was injected into a thin-light path horizontal cuvette (BioLogic) and placed on the JST-100 in vertical mode. Cells were illuminated for 2 min with a 500 µmol photon $m^{-2} s^{-1}$ red light (630 nm) to reach stable photosynthetic gas exchange reached before recording absorbance changes for ECS measurement and PMF size and partitioning determination. After 5 seconds of initiation of the recording, light was turned off and absorbance changes were recorded for 30 more seconds until full recovery of the signal. ECS signal was calculated as the difference between absorbance changes measured

at 520 and 545 nm. For each biological replicate, 3 technical replicates were taken and averaged. pH gradient and electric field ($\Delta\Psi$) composition of the ECS was calculated as described[57]. Total PMF size was calculated as $\Delta pH + \Delta\Psi$.

Chlorophyll fluorescence and NPQ measurements

Chlorophyll fluorescence was measured using a pulsed amplitude modulation (PAM) fluorimeter (Dual-PAM 100, Walz) on the MIMS chamber as described[50] using green actinic light (2,000 µmol photon m^{-2} s^{-1}; green LEDs). Red saturating flashes (8,000 µmol photons m^{-2} s^{-1}, 600 ms) were delivered to measure the initial maximal fluorescence yield (F_M) (in dark-acclimated samples) and then every 30 s to measure F'_M (upon actinic light exposure). NPQ was calculated as $(F_M - F'_M)/F'_M$.

77K chlorophyll fluorescence spectra were measured on whole cells using an Ocean Insight FLAME-X optical fiber fluorescence spectrophotometer. About 200 µl of cell culture at around 10 µg chlorophyll per ml was fast frozen in liquid nitrogen. The excitation wavelength was 440 nm, and excitation and emission slits were 10 and 5 nm, respectively.

O_2 exchange measurement and calculations of electron fluxes though alternative pathways depending on C_i concentration

O_2 exchange was measured by MIMS using ^{18}O-enriched O_2 as described[49] on *pgrl1*, *flvB* and their respective control strains 137AH and CC-4533. Upon illumination, the C_i was depleted by photosynthesis, allowing to determine gas exchange rates at various C_i concentrations[58]. O_2 exchange rates were averaged from three biological replicates (Extended Data Fig. 8) and used to calculate the maximal capacity of each pathway. As the CCM functioning is not affected in *pgrl1* (Fig. 1), we considered that the increase in O_2 uptake rates between *pgrl1* and its control strain (O_2 difference$_{pgrl1}$) (Extended Data Fig. 8) reflects the additional electron flux to O_2 compensating the absence of PGRL1-mediated CEF. As CEF is 1.5 times less efficient than PCEF to generate a proton gradient[59], CEF was calculated as equal to 1.5 × O_2 difference$_{pgrl1}$. The FLV-mediated PCEF was calculated as the difference in O_2 uptake rates between CC-4533 and *flvB* (Extended Data Fig. 8). CMEF was calculated as the light-induced O_2 uptake remaining in the *flvB* mutant (Extended Data Fig. 8). To determine the contribution of alternative electron pathways to CCM energizing as compared to CO_2 fixation, CEF was normalized to net O_2 evolution measured in *pgrl1* and both PCEF and CMEF were normalized to net O_2 evolution in *flvB*.

Material availability

All biological material described in this study is available upon request.

Reporting summary

Further information on research design is available in the Nature Research Reporting Summary linked to this paper.

Data availability

Genes studied in this Article can be found on https://phytozome-next.jgi.doe.gov/ under the loci Cre12.g531900 (*FLVA*), Cre16.g691800 (*FLVB*), Cre07.g340200 (*PGRL1*), Cre16.g662600 (*BST1*), Cre16.g663400 (*BST2*) and Cre16.g663450 (*BST3*).

49. Burlacot, A., Burlacot, F., Li-Beisson, Y. & Peltier, G. Membrane inlet mass spectrometry: a powerful tool for algal research. *Front. Plant. Sci.* **11**, 1302 (2020).
50. Burlacot, A. et al. Flavodiiron-mediated O_2 photoreduction links H_2 production with CO_2 fixation during the anaerobic induction of photosynthesis. *Plant Physiol.* **177**, 1639–1649 (2018).
51. Burlacot, A., Richaud, P., Gosset, A., Li-Beisson, Y. & Peltier, G. Algal photosynthesis converts nitric oxide into nitrous oxide. *Proc. Natl Acad. Sci. USA* **117**, 2704–2709 (2020).
52. Desplats, C. et al. Characterization of Nda2, a plastoquinone-reducing type II NAD(P)H dehydrogenase in *Chlamydomonas* chloroplasts. *J. Biol. Chem.* **284**, 4148–4157 (2009).
53. Yamano, T. et al. Light and low-CO_2-dependent LCIB–LCIC complex localization in the chloroplast supports the carbon-concentrating mechanism in *Chlamydomonas reinhardtii*. *Plant Cell Physiol.* **51**, 1453–1468 (2010).
54. Moroney, J. V. et al. Isolation and characterization of a mutant of *Chlamydomonas reinhardtii* deficient in the CO_2 concentrating mechanism. *Plant Physiol.* **89**, 897–903 (1989).
55. Gerster, R. An attempt to interpret the kinetics of isotope exchange between $C^{18}O_2$ and the water of a leaf: experiments in the dark. *Planta* **97**, 155–172 (1971).
56. Silverman, D. N. In *Methods in Enzymology* Vol. 87 (ed. Purich, D. L.) 732–752 (Academic Press, 1982).
57. Cruz, J. A., Sacksteder, C. A., Kanazawa, A. & Kramer, D. M. Contribution of electric field (Δψ) to steady-state transthylakoid proton motive force (*pmf*) in vitro and in vivo. control of *pmf* parsing into Δψ and ΔpH by ionic strength. *Biochem.* **40**, 1226–1237 (2001).
58. Douchi, D. et al. Membrane-inlet mass spectrometry enables a quantitative understanding of inorganic carbon uptake flux and carbon concentrating mechanisms in metabolically engineered cyanobacteria. *Front. Microbiol.* **10**, 1356–1356 (2019).
59. Kramer, D. M. & Evans, J. R. The importance of energy balance in improving photosynthetic productivity. *Plant Physiol.* **155**, 70–78 (2011).

Acknowledgements This work was supported by the A*MIDEX (ANR-11-IDEX-0001-02) project and by the ANR OTOLHYD. A.B. acknowledges support from the Carnegie Institution for Science. O.D. is the recipient of a PhD grant awarded to Y.L-.B. We thank A. Grossman for use of the JTS-100; G. Peers for stimulating discussion; K. K. Niyogi and M. Iwai for critical reading of the manuscript; J. V. Moroney for the *bsti-1* mutant; L. Mackinder for the BST3 antibody; and H. Fukuzawa for the LCIA and LCI1 antibodies. We gratefully acknowledge the contributions of S. Moulin for artistic drawings in Fig. 4, S. Blangy for LCIC antibody preparation, E. Calikanzaros and V. Epting for technical assistance, and A. Gosset for performing genetic crosses of *flvB* and *pgrl1* mutants. The authors acknowledge the European Union Regional Developing Fund, the Region Provence Alpes Côte d'Azur, the French Ministry of Research, and the CEA for funding the HelioBiotec platform.

Author contributions A.B. and G.P. designed the research; A.B., O.D., P.A., S.C. and G.P. performed research; A.B. and G.P. contributed new reagents and analytic tools; A.B. and G.P. analysed data; A.B. and G.P. wrote the paper with input from Y.L.-B.

Competing interests The authors declare no competing interests.

Additional information
Supplementary information The online version contains supplementary material available at https://doi.org/10.1038/s41586-022-04662-9.

Correspondence and requests for materials should be addressed to Gilles Peltier.

Peer review information *Nature* thanks Cornelia Spetea Wiklund and the other, anonymous, reviewers for their contribution to the peer review of this work. Peer reviewer reports are available.